Thermal Science and Engineering Progress 45 (2023) 102126

Contents lists available at ScienceDirect

Thermal Science and Engineering Progress

journal homepage: www.sciencedirect.com/journal/thermal-science-and-engineering-progress

Lattice Boltzmann simulation of natural convection heat transfer phenomenon for thermal management of multiple electronic components

Hamza Faraji [a,*], Mohamed Teggar [b], Adeel Arshad [c,*], Müslüm Arıcı [d], El Mehdi Berra [e], Khadija Choukairy [f]

[a] LISA Laboratory, National School of Applied Sciences, Cadi Ayyad University, Marrakech, Morocco
[b] Laboratory of Mechanics, Amar Telidji University, 03000, Laghouat, Algeria
[c] Environment and Sustainability Institute (ESI), Faculty of Environment, Science and Economy, University of Exeter, Penryn Campus, Cornwall, TR10 9FE, United Kingdom
[d] Mechanical Engineering Department, Engineering Faculty, Kocaeli University, Kocaeli, 41001, Turkey
[e] Renewable Energy & Dynamic Systems Laboratory, Physics Department, Faculty of Sciences Ain Chock, Hassan II University, Casablanca, Morocco
[f] Laboratory of Computer and Mathematical Process Engineering, National School of Applied Sciences, Moulay Slimane University, Khouribga, Morocco

ARTICLE INFO

Keywords:
Heat sink
Lattice Boltzmann method
Natural convection
Nusselt number
Thermal management

ABSTRACT

Thermal management of electronic components is becoming a vital necessity in view of the rapid development of electronics technology. It is a concern imposed by the miniaturization of electronic chipsets. The present work addresses this issue numerically, using the lattice Boltzmann method (LBM). It consists of an air-filled heat sink containing multiple protruding electronic components. The problem is modelled using 2D continuity, momentum, and energy conservation equations. The thermal and dynamic fluid flow are analysed for various enclosure inclinations (0°, 45°, and 90°) and Rayleigh numbers ($Ra = 10^3 - 10^6$). A twin protruding heat sources are considered at the bottom wall. The top cold wall can be at a uniform temperature (case 1) or consisting of two protruding sinks maintained at a constant temperature (case 2). The results showed that the maximum heat transfer rate corresponding to Nusselt number ($\overline{Nu} = 5.51$) is achieved for $Ra = 10^6$ on the hot wall for the horizontal cavity in case 1, illustrating the cavity with top cold uniform wall. Indeed, the heat transfer is improved by 80% by varying the Rayleigh number (Ra) from 10^3 to 10^6. Furthermore, for case 2 with a twin cold protruding, a quite complicated heat transfer behaviour is observed on the hot wall. For $Ra > 10^6$, the horizontal cavity outperforms the other cavities in terms of heat transfer rate, however the horizontal position is the less performant for $Ra < 10^4$. With a horizontal disposition and $Ra = 10^6$, the heat exchange ratio is improved by 32.32% in case 2 compared to case 1. The outcomes of this study provide insights into design and implementation of natural convection cooling solutions for electronic devices, which can have significant practical implications in various industries.

1. Introduction

The natural convection heat transfer is a fundamental heat transfer process that occurs in many natural and engineering systems. It arises from the density differences in fluids that are caused by temperature variations, leading to buoyancy forces that drive fluid motion [1]. Natural convection (NC) heat transfer mode has been extensively studied for its application in various fields such as building ventilation, geothermal energy systems, and cooling of electronic components [2–4]. In particular, thermal management of electronic components has become a critical issue due to the increasing power density and miniaturization of electronic devices, since excessive heat generated may cause degradation of device performance and even permanent damage [5,6]. Therefore, effective cooling strategies are essential to maintain the reliability and longevity of electronic devices. The NC heat transfer has emerged as a promising mode for thermal management of electronic components due to its simplicity and low cost. Compared to forced convection heat transfer cooling techniques that require external power sources [7], NC heat transfer cooling technique utilizes the inherent buoyancy forces within the fluid, making it a more energy-efficient solution. Moreover, it can operate without any moving parts, making it

* Corresponding authors.
E-mail addresses: hamza.faraji@uca.ac.ma (H. Faraji), a.arshad@exeter.ac.uk, adeel_kirmani@hotmail.com (A. Arshad).

https://doi.org/10.1016/j.tsep.2023.102126
Received 27 April 2023; Received in revised form 31 August 2023; Accepted 12 September 2023
Available online 17 September 2023
2451-9049/Crown Copyright © 2023 Published by Elsevier Ltd. This is an open access article under the CC BY license (http://creativecommons.org/licenses/by/4.0/).

Nomenclature

c_s	lattice sound speed $= \frac{c}{\sqrt{3}}$, (m/s)
c_k	discrete lattice speed, (m/s)
F_k	external force (buoyancy force)
f_k	single particle distribution function for density
g	gravitational acceleration, (m/s^2)
g_k	single particle distribution function for temperature
H	height, (m)
h_b	electronic component heigth, (m)
k	thermal conductivity, (W/mK)
L	length, (m)
L_b	electronic component length, (m)
Nu	Nusselt number
NC	natural convection
Pr	Prandtl number
P	dimensionless pression
p	pression, (Pa)
Ra	Rayleigh number
t	time, (s)
T	dimensionless temperature
U, V	dimensionless components of macroscopic velocity
u, v	components of macroscopic velocity, (m/s)
w_k	weighting factor
x, y	Cartesian coordinate, (m)

Scripts

c	cold
eq	equilibrium state
f	base fluid
h	hot

Greek symbols

α	thermal diffusivity, (m^2/s)
β	thermal expansion, (1/K)
$\delta x, \delta y$	lattice space steps, (m)
ρ	density, (kg/m^3)
ϑ	macroscopic viscosity
η	perpendicular to the wall
Ω	tilt angle, (°)
τ	relaxation time
Δt	lattice time step

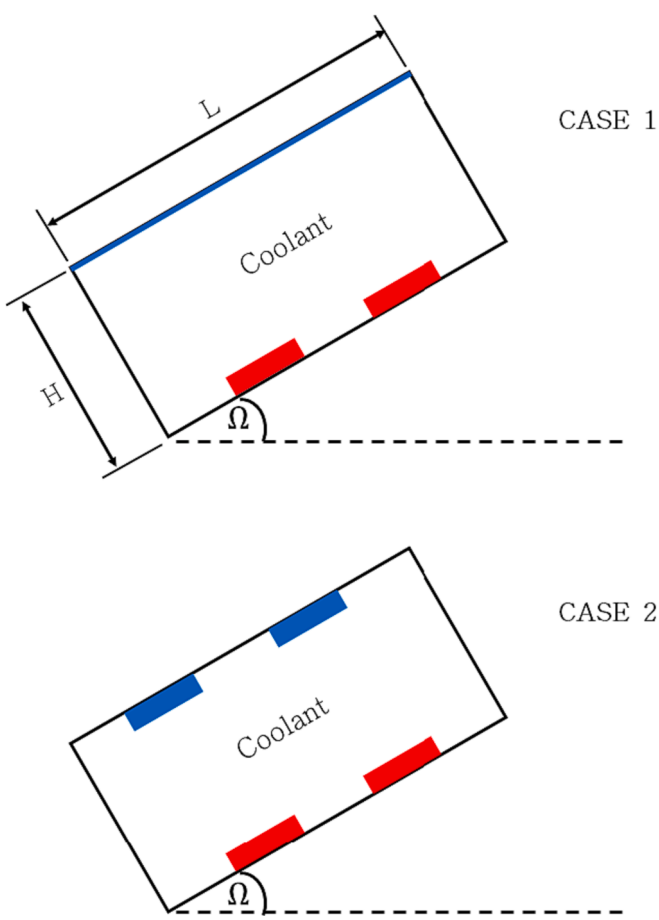

Fig. 1. Schematic of the physical model.

more reliable and quieter than forced convection cooling techniques [8,9]. In recent years, heat transfer by NC has been studied in enclosures containing a fluid [10]. These enclosures may involve heating blocks or not. This is a research focus, which has received increasing attention.

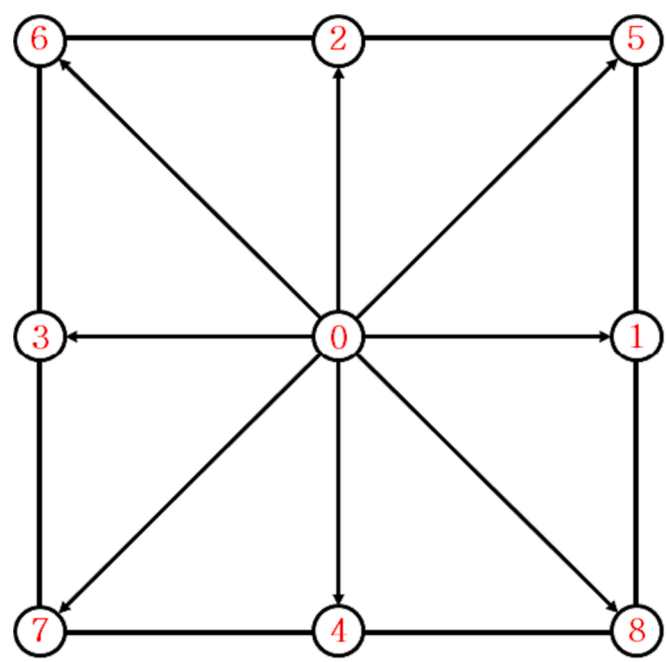

Fig. 2. Discrete velocity vectors for D2Q9.

Table 1
Results dependence on grid size.

	ψ $Ra = 10^3$, $\Omega = 90^\circ$	Deviation (%)	ψ $Ra = 10^6$, $\Omega = 0^\circ$	Deviation (%)
200 × 100	0.445	–	19.143	–
300 × 150	0.542	17.89	21.654	11.59
400 × 200	0.569	4.74	22.777	4.93
500 × 250	0.563	1.05	23.103	1.41

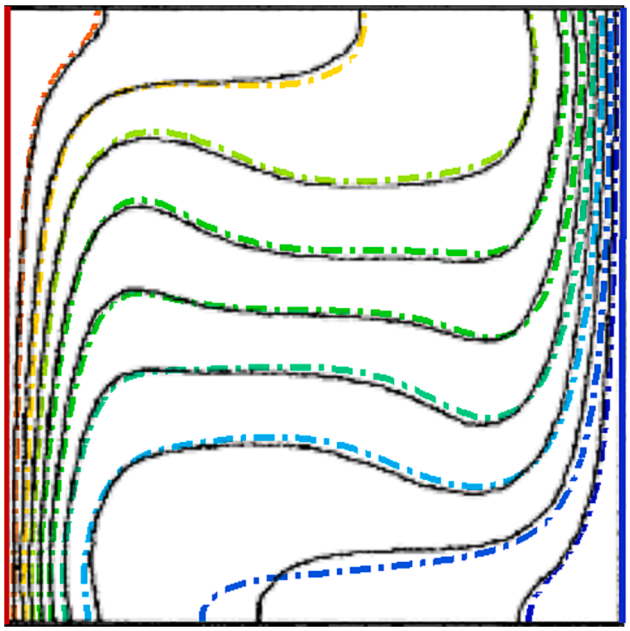

Fig. 3. Substantiation of the accuracy of our code by comparison between our numerical results (dashed) and those obtained by De Vahl Davis [57] (solid) in terms of isotherms for $Ra = 10^5$.

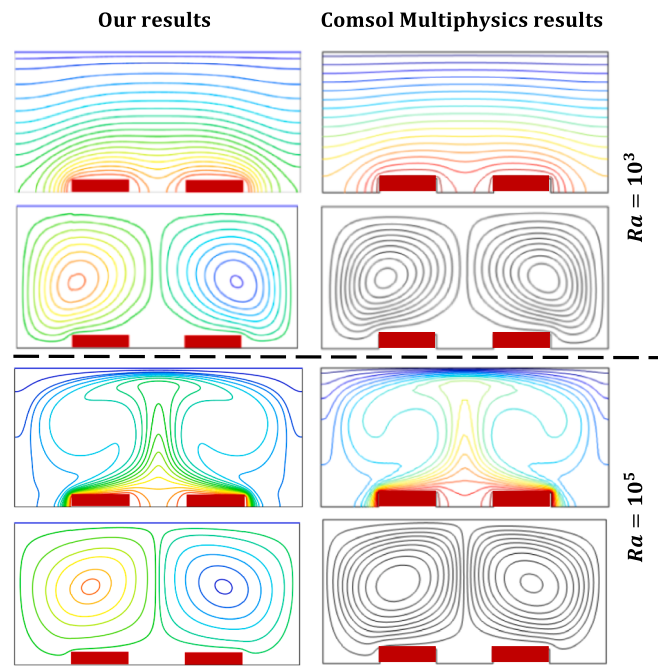

Fig. 4. Substantiation of the accuracy of our code against numerical results obtained by COMSOL Multiphysics software in terms of isotherms (top) and streamlines (bottom) for $Ra = 10^3$ and $Ra = 10^5$.

Table 2
Comparison of average *Nu* values.

CFD approach:	Our results LBM	De Vahl Davis [57] FDM	Khanafer et al. [58] FVM	Fusegi et al. [59] FDM
$Ra = 10^3$	1.09	1.11	1.11	1.10
$Ra = 10^5$	4.48	4.51	4.52	4.64
$Ra = 10^6$	8.77	8.79	8.82	9.01

Table 3
Comparison maximum dimensionless velocities along the vertical and horizontal centerline.

		Our results	De Vahl Davis [57]	Deviation (%)
$Ra = 10^3$	U_{max}	3.46	3.64	4.94
	V_{max}	3.52	3.69	4.60
$Ra = 10^5$	U_{max}	36.09	34.73	3.76
	V_{max}	69.35	68.59	1.09
$Ra = 10^6$	U_{max}	64.81	64.63	0.27
	V_{max}	218.18	219.36	0.53

Heat sinks designed for thermal management of electronic components and other industrial applications are characterized by the omnipresence of the NC heat transfer mechanism. Numerous research works have been dedicated to understanding this mechanism. Ma et al. [11] numerically studied NC heat transfer by lattice Boltzmann method (LBM). The outcomes evidenced increasing average Nusselt number (*Nu*) with incrementing Rayleigh number (*Ra*). Furthermore, it was shown that for $Ra \geq 10^4$, the heat transfer enhancement became increasingly significant. Franco et al. [12] studied NC heat transfer in a square enclosure under the effects of several conducting blocks. An increase in the average Nusselt number by a factor of four was reported with increasing the *Ra*. Similarly, the NC heat flow was hindered by the increase in the number of blocks. Khan et al. [13] developed simulations for enhancing NC heat transfer through fluids. The major interest was given to the type of the used base fluid as an influential parameter. Wang et al. [14] numerically studied the phenomenon of NC heat loss in an isothermal cavity. The impact of the surface temperature, tilt angle, and opening ratio was analysed. It was shown that the heat loss by NC increased with increasing the surface temperature and opening ratio. However, an increase in the tilt angle decreased the heat loss. In addition, it was claimed that increasing the air velocity in the enclosure resulted in a rise in the heat loss. Farahani et al. [15] studied the NC heat transfer in a cavity of rectangular geometry. The effect of adding an obstacle on the heat transfer was analysed. It was found that the obstacle dimensions have a major effect on the heat transfer within the cavity. Furthermore, a clockwise rotation of the obstacle was accompanied by an increase in heat transfer and the latter was decreased in the case of a counterclockwise rotation. Baghsaz et al. [16] numerically investigated the NC heat transfer in a nanofluid filled cavity considering Ra values ranging from 10^4 to 10^7. It was shown that the heat transfer was improved by increasing Ra. However, the sedimentation phenomenon of nanoparticles was decreased the *Nu*. Gawas and Patil [17] evaluated NC heat transfer with thermal diffusion in an inclined cavity. It was shown that heat transfer developed by increasing the tilt angle (counterclockwise) and increased the thermal diffusion. Selimefendigil and Öztop [18]studied an enclosure containing or not containing obstacles of various geometries. It was found that the existence of obstacles within the enclosure decreased the heat transfer rate. Sheikholeslami et al. [19] investigated the NC heat transfer in an inclined cavity with curved boundaries. It was shown that the enclosure's orientation and its aspect ratio were also determining factors, in addition to *Ra*. Indeed, the maximal Nu was found with the inclination of 0° for $Ra = 10^3$. For the rest of *Ra* values, the maximal heat transfer rate was observed for an inclination of 30°. In this regard, Ma et al. [20] performed numerical simulations of NC heat transfer in an enclosure containing heating obstacle, and the heat transfer was reported to be significant in a narrower enclosure. Daghab et al. [21] performed simulations on NC heat

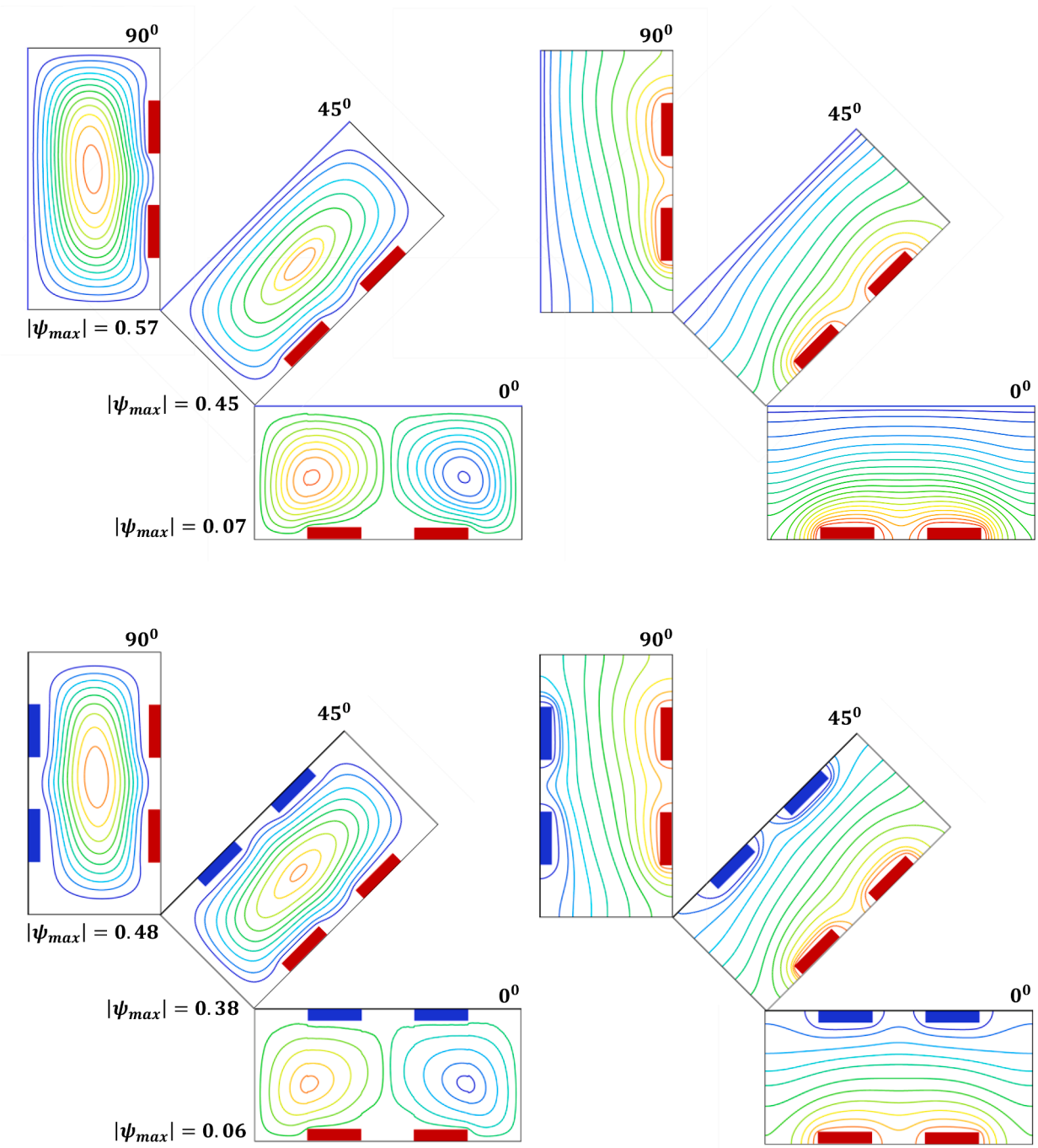

Fig. 5. Isotherms (right) and streamlines (left) obtained for case 1 (top) and case 2 (bottom) and $Ra = 10^3$.

transfer for thermal management of a heat source, the finite volume method (FVM) was used for simulations. The results indicated improved cooling performance when *Ra* was incremented. Hidki et al. [22] numerically investigated the NC in a square enclosure in the presence of heating elements by using the FVM. The maximum temperature decreased, and heat transfer increased by boosting *Ra*. Arroub et al. [23] developed a work on numerical modelling on heat transfer with laminar flow using the FVM. It was shown that the best cooling inside the cavity was achieved by using a rectangular enclosure of an aspect ratio of 2. Benhamou et al. [24] evaluated the free convection heat transfer phenomena in an air-filled enclosure and reported that the fluid could exchange its heat in a uniform way with the hot surfaces of an obstacle for $Ra = 10^3$. For higher values i.e., $Ra \geq 10^4$, this heat exchange was found to be important on the obstacle's lower face compared to the other faces. Saha [25] has numerically studied the NC heat transfer in a trapezoidal enclosure. Different inclinations and aspect ratios of the enclosure were considered. Incrementing the aspect ratio of the enclosure resulted in a large thermally stratified region. In addition, increasing the angle of inclination between two non-parallel sidewalls resulted in stronger convection. Zemani and Sabeur [26] studied NC in an air-filled enclosure bounded by partially active sidewalls. The enclosure contained a partition attached to the hot wall and different positions were assigned to this partition to evaluate their effect. The results showed decreasing heat transfer with the increase in the partition length particularly for a value of L/2. Moreover, a maximum value of the average Nu was pointed out in the case of a middle-middle arrangement.

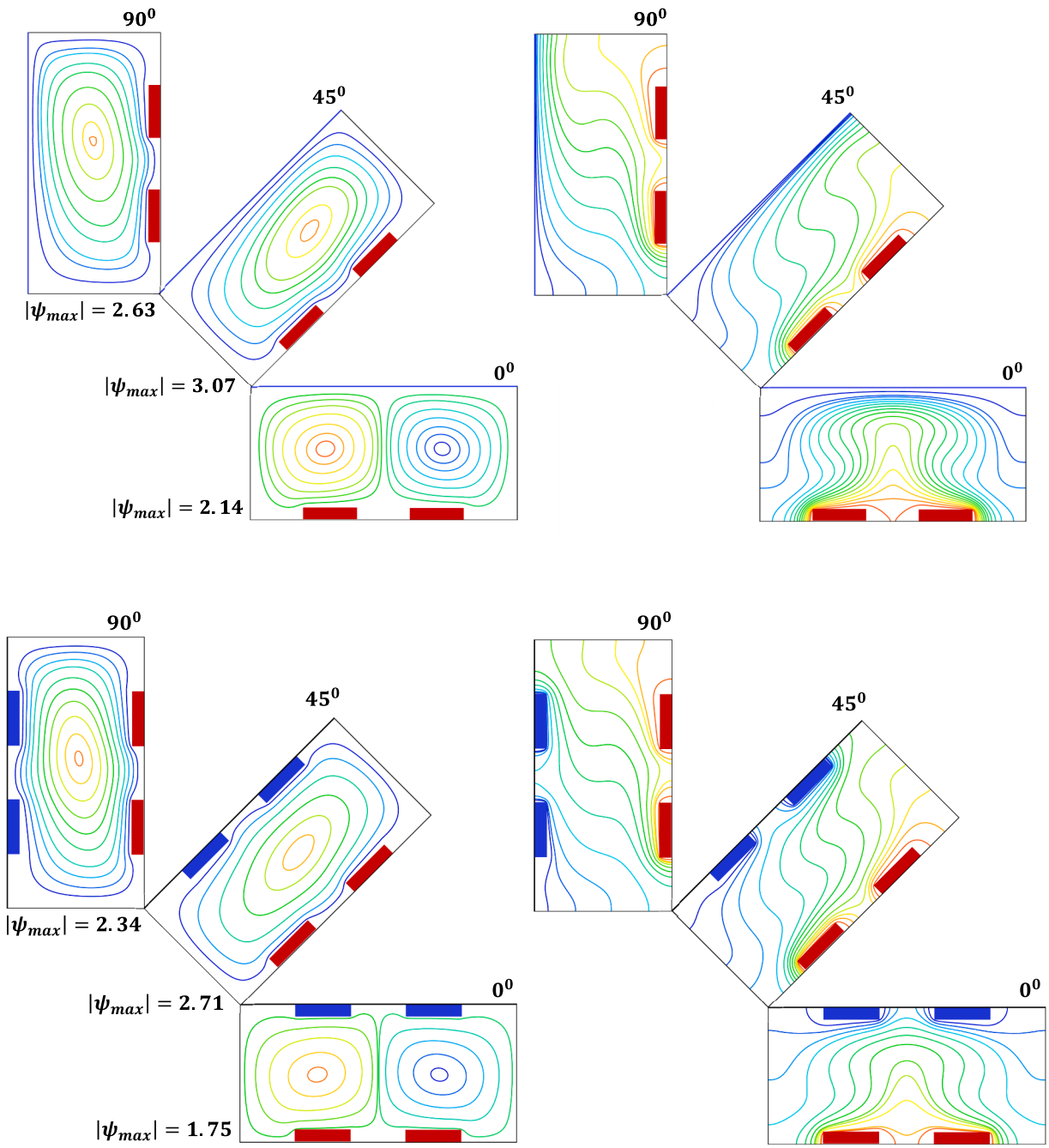

Fig. 6. Isotherms (right) and streamlines (left) obtained for case 1 (top) and case 2 (bottom) and $Ra = 10^4$.

Alinejad and Esfahani [27] conducted the LBM simulation of electronic board using different shapes of obstacles using *Ra* range of 250 to 1000 at $Pr = 0.71$. The results showed that with the increase of *Ra* removed the higher quantity of energy from the obstacles. It was also found that distance between the obstacles made the flow deviated and accelerated. Further, they investigated the three-dimensional turbulent convection heat transfer around an isothermal cylinder using LBM simulation under *Ra* (10^3 to 10^9) and aspect ratio (0.5 to 2) [28,29]. The results showed the vortex shedding maps in all cases and revealed the maximum heat transfer of the triangular unit at stagnation point of the cylinder. Also, the mean *Nu* of upstream cylinder was higher in comparison to the downstream cylinder [30]. Djebali and Ferhi [31,32] investigated the magnetohydrodynamics (MHD) heat transfer enhancement and entropy generation using LBM of a micro-open tall cavity under the effect of magnetic field and sinusoidal heating. The authors studied the flow patterns, heat transfer characteristics and irreversibility patterns by varying *Ra* (102–104), *Ku* (0–0.1), *Ha* (0–80) and volume fraction (0–0.04 %). The authors found that the rarefaction phenomenon played a significant role in the intensification of the heat transfer. Ferhi et al. [33,34] conducted the LBM to study the natural conjugate heat transfer and entropy generation of partially heated and cooled cavity filled with MWCNT/water, Ag-MgO/water and Al_2O_3/water based nanofluid under uniform magnetic field. The authors found that heat transfer was increased at low *Ra* with solid volume fraction and entropy generation remained constant. Furthermore, with the increase of *Ha* heat transfer and entropy generation both were decreased, whereas *Be* was increased. The various applications and challenges of NC heat transfer with complex enclosures were discussed in [35–37].

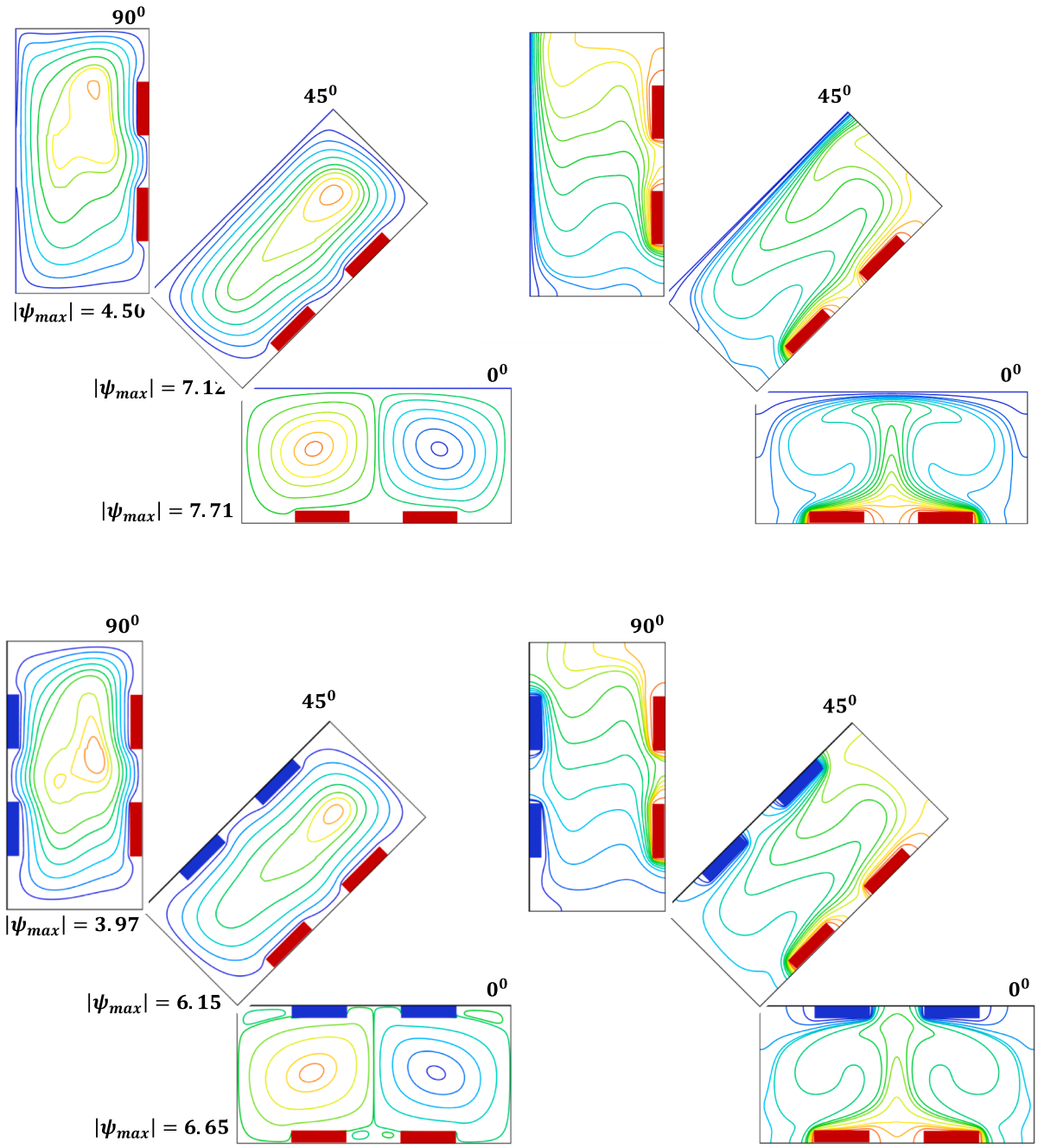

Fig. 7. Isotherms (right) and streamlines- (left) obtained for case 1 (top) and case 2 (bottom) and $Ra = 10^5$.

Most of the studies published in the literature treat the phenomenon of NC heat transfer using classical numerical computational methods. Indeed, we find works based on the finite element method (FEM) [38–40], the finite difference method (FDM) [41–43] and the finite volume method (FVM) [44,45]. The last decade has been characterized by the appearance of a powerful and efficient numerical tool for the treatment of heat transfer problems even with higher complexity, which includes the lattice Boltzmann method (LBM) [46–48].

Most of the studies deal with heat transfer problems by NC in enclosures of different geometries, heated/cooled by isothermal walls. Few studies have focused on thermal management of electronic components that are generally protruding solved by LBM. To the best of the authors' knowledge, NC heat transfer inside an enclosure containing multiple protruding electronic components simultaneously cold and hot in the same enclosure has not yet been addressed using the LBM. Therefore, the originality of the present work lies in the fact that it deals with the phenomenon of conjugate heat transfer in a rectangular enclosure filled with air for thermal management of multiple electronic components with different cooling strategies via the LBM. To this end, a detailed study is carried out to unveil the effect of the adopted cooling strategy, inclination of the enclosure and Ra on the heat transfer and fluid flow structures.

2. Physical and mathematical model

2.1. Physics of the problem

The present physical problem is studied for the purpose of the

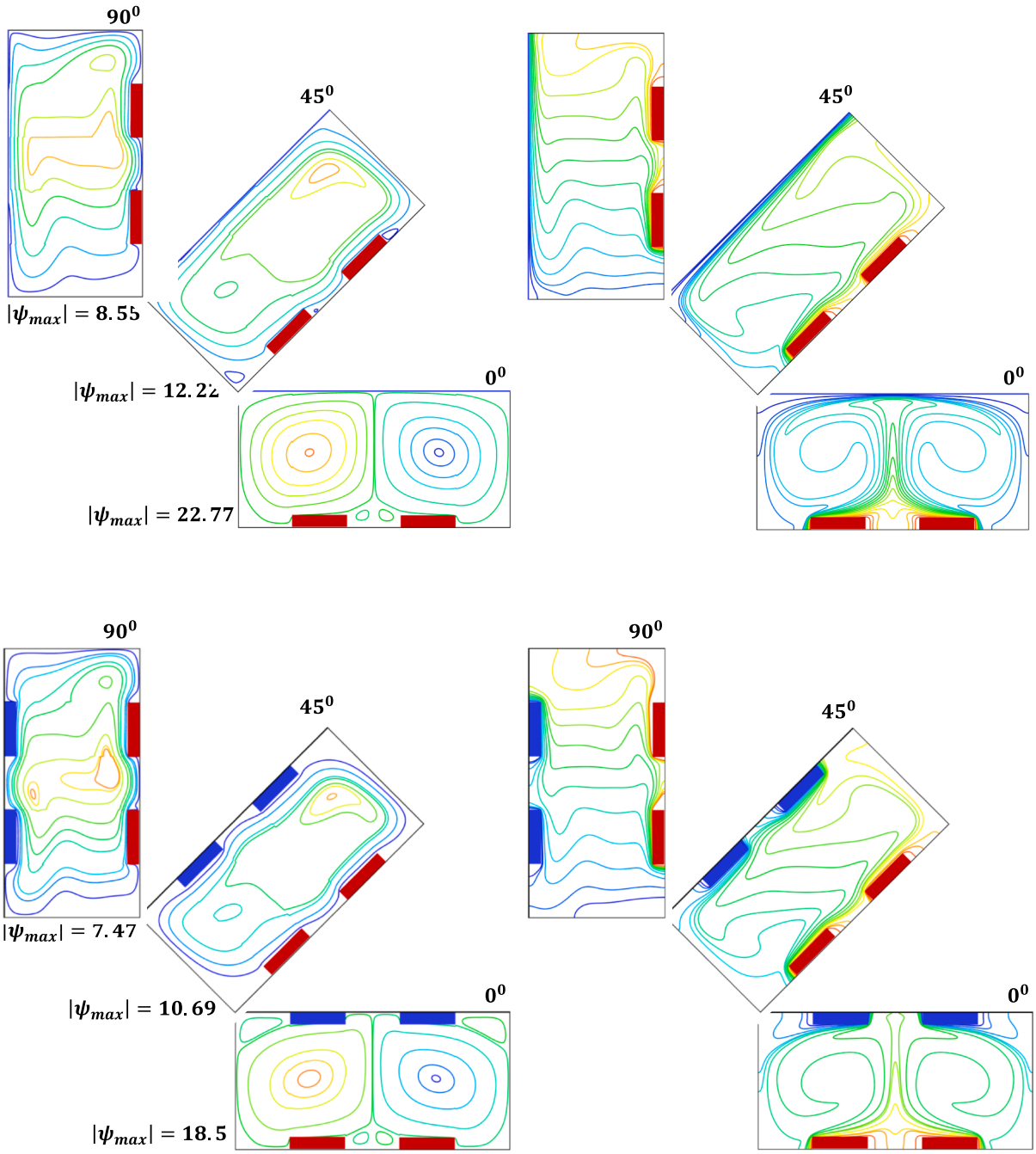

Fig. 8. Isotherms (right) and streamlines (left) obtained for case 1 (top) and case 2 (bottom) and $Ra = 10^6$.

thermal management of electronic components. The conjugate heat transfer by conduction and NC heat transfer in a rectangular enclosure filled with air ($Pr = \frac{\vartheta}{\alpha} = 0.71$) [49] has been numerically studied by using the LBM method. The enclosure contains two protruding heat sources modelling electronic components maintained at constant temperatures of T_h: "ON" state. Two techniques for cooling these electronic components have been adopted. The enclosure could be cooled by either a cold wall maintained at a uniform constant temperature T_c (case 1) or two heat sinks at T_c (cases 2): "OFF" state. Fig. 1 shows, in detail, the geometry studied, and the two cases treated along with their boundary conditions.

The present paper develops a 2D investigation in order to simulate, by using LBM, the conjugate heat transfer in an air-filled rectangular enclosure, which is heated by a discrete pair of protuberant sources simulating electronic components and cooled either by uniform cold wall or a discrete pair of sinks while all the other walls of the cavity are adiabatic, as shown in Fig. 1. The enclosure is of height H and length L inclined by an angle Ω. Each electronic component has a height of h_b and a length of L_b. The proposed mathematical model is established based on the physics of the current problem. This model is based on Navier–-Stokes Equations. For a computational resolution of this problem, the following assumptions are adopted:

- The working fluid flow is supposed to be laminar, incompressible, and Newtonian.
- No viscous dissipation effects in the energy equation.

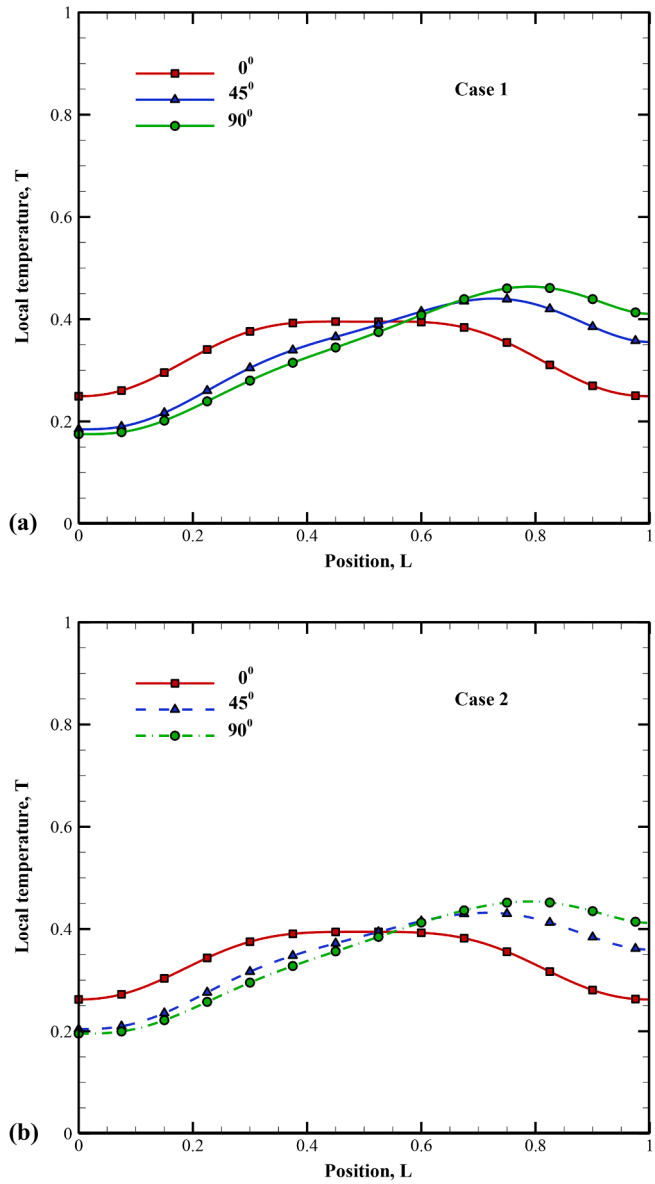

Fig. 9. Local temperature distribution along the central line for $Ra = 10^3$.

- Thermal radiation is neglected.
- All thermophysical properties are assumed to be constant and the Boussinesq approximation is adopted to control density variation.

The system of non-dimensional equations governing the physical problem described above, based on simplifying assumptions, can be expressed as follows:

$$\frac{\partial U}{\partial X}+\frac{\partial V}{\partial Y}=0 \tag{1}$$

$$U\frac{\partial U}{\partial X}+V\frac{\partial U}{\partial Y}=-\frac{\partial P}{\partial X}+Pr\left(\frac{\partial^2 U}{\partial X^2}+\frac{\partial^2 U}{\partial Y^2}\right)+Ra.Pr.T.\sin(\Omega) \tag{2}$$

$$U\frac{\partial V}{\partial X}+V\frac{\partial V}{\partial Y}=-\frac{\partial P}{\partial Y}+Pr\left(\frac{\partial^2 V}{\partial X^2}+\frac{\partial^2 V}{\partial Y^2}\right)+Ra.Pr.T.cos(\Omega) \tag{3}$$

$$U\frac{\partial T}{\partial X}+V\frac{\partial T}{\partial Y}=\frac{\partial^2 T}{\partial X^2}+\frac{\partial^2 T}{\partial Y^2} \tag{4}$$

The following non-dimensional parameters are defined as follow:

$$X=\frac{x}{H}$$
$$Y=\frac{y}{H}$$
$$U=\frac{uH}{\alpha}$$
$$V=\frac{vH}{\alpha}$$
$$P=\frac{p}{\rho(\alpha/H)^2}$$
$$T=\frac{T_0-T_C}{T_H-T_C}$$
$$Ra=\frac{g\beta(T_H-T_C)H^3}{\alpha\vartheta}$$

2.2. Lattice Boltzmann method

The phenomena of conjugate NC heat transfer and fluid flow are generally governed by the Navier-Stokes equations. The numerical resolution of these equations could be achieved by using different numerical methods. Among them is the LBM which is recently developed to avoid the iterative resolution at each time step adopted by traditional numerical methods. Indeed, the LBM has been found to be efficient and simple in terms of computation and formulation both when it first appeared [50,51] and after modifications and improvements [52,53]. The LBM is based on two distribution functions: one for the dynamic field $f_k(x,t)$ and the other for the thermal field $g_k(x,t)$. A 2D LBM-based model with nine velocities (LBM-D2Q9) [54] is used as shown in Fig. 2. The entire computational domain was subject to a uniform mesh, in both directions, with $\delta x = \delta y$.

2.2.1. LBM for fluid flow

By adopting the single relaxation time approximation, known as the Bhatnager, Gross, and Krook (BGK) approximation and according to the D2Q9 model [54], the lattice Boltzmann equation for velocity field in the k direction, is given by:

$$f_k(x+c_k\Delta t,t+\Delta t)-f_k(x,t)=-\frac{f_k(x,t)-f_k^{eq}(x,t)}{\tau}+\Delta t.F_k.c_k \tag{5}$$

c_k is defined by:

$$c_k=\begin{cases} c_0=(0,0);\ k=0 \\ c_i=c(\cos\theta_k,\sin\theta_k);\ k=1,2,3,4;\ \theta_k=(i-1)\pi/2 \\ c_i=c\sqrt{2}\,(\cos\theta_k,\sin\theta_k);\ k=5,6,7,8;\ \theta_k=(i-5)\pi/2+\pi/4 \end{cases} \tag{6}$$

c and Δt are taken equal to unity in the simulations. τ is expressed as follow:

$$\tau=\frac{\vartheta}{c_s^2\Delta t}+\frac{1}{2} \tag{7}$$

where c_s is given by $\frac{c}{\sqrt{3}}$.

The local equilibrium distribution function f_k^{eq} depends appropriately on the local hydrodynamic properties. It is given by:

$$f_k^{eq}=w_k\rho\left[1+3\frac{c_k u^{eq}}{c^2}+\frac{9}{2}\frac{(c_k u^{eq})^2}{c^4}-\frac{3}{2}\frac{u^{eq}u^{eq}}{c^2}\right] \tag{8}$$

w_k are given by:

$$w_k=\begin{cases} \frac{4}{9};\ k=0 \\ \frac{1}{9};\ k=1,2,3,4 \\ \frac{1}{36};\ k=5,6,7,8 \end{cases} \tag{9}$$

The summation of moments in the velocity space is used to evaluate the following hydrodynamic quantities:

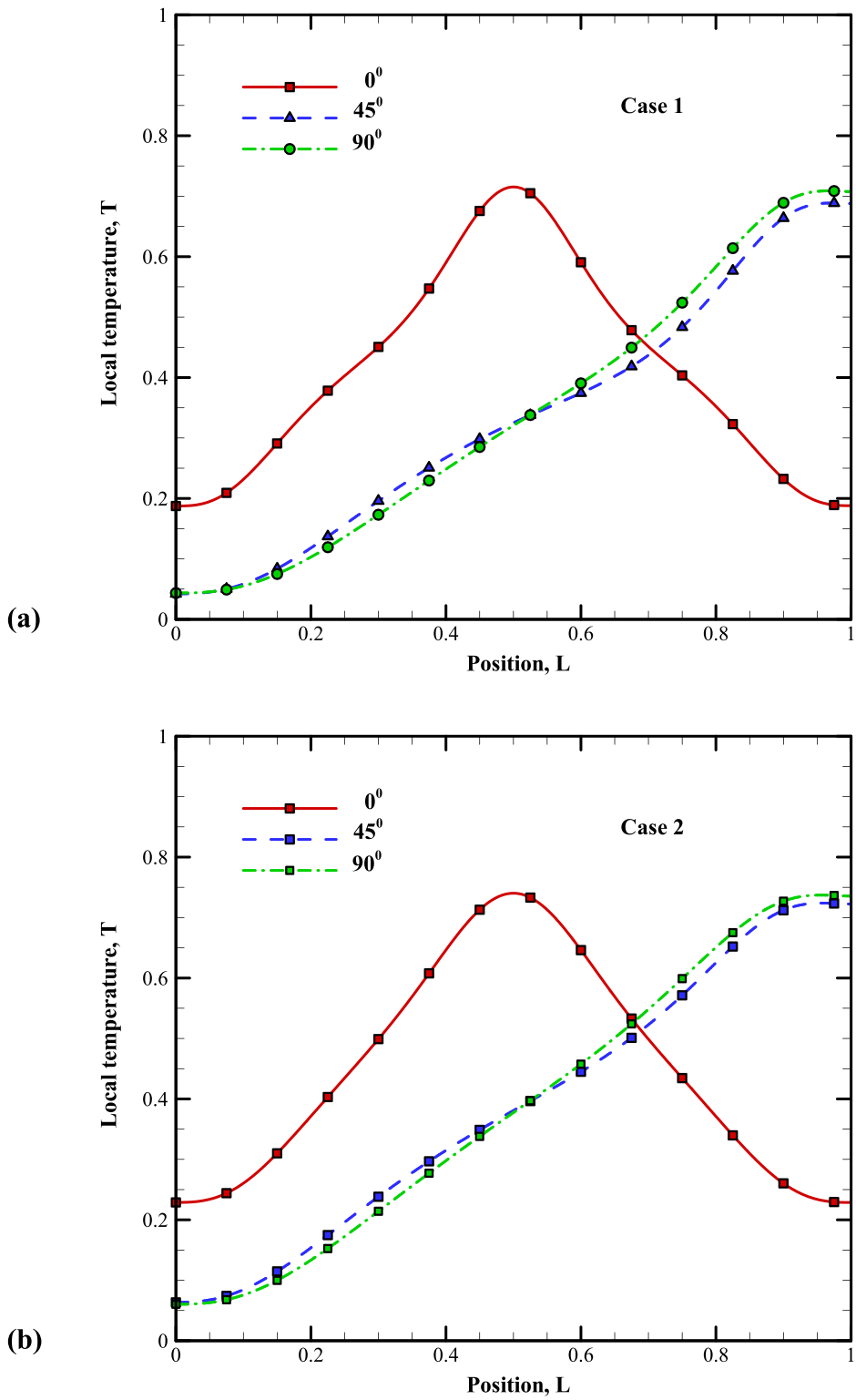

Fig. 10. Local temperature distribution along the central line for $Ra = 10^4$.

$$\rho(x,t) = \sum_{k=0}^{8} f_k(x,t) \tag{10}$$

$$\rho u(x,t) = \sum_{k=0}^{8} c_k f_k(x,t) \tag{11}$$

2.2.2. LBM for heat transfer

The LBM mathematical modelling of the thermal behaviour is introduced in this sub-section. The lattice Boltzmann equation for temperature field, under the BGK approximation, is given by [55]:

$$g_k(x + c_k\Delta t, t + \Delta t) - g_k(x,t) = -\frac{1}{\tau}\left[g_k(x,t) - g_k^{eq}(x,t)\right] \tag{12}$$

Since the flow is incompressible, the compression work resulting

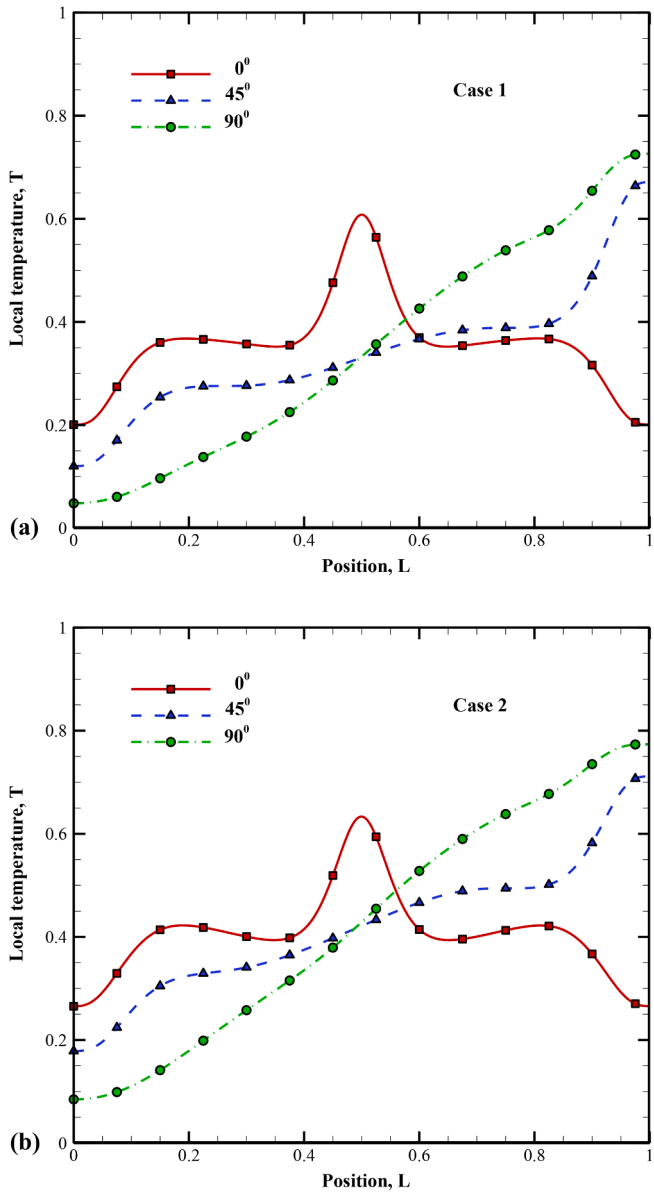

Fig. 11. Local temperature distribution along the central line for $Ra = 10^5$.

from pressure and heat dissipation can be neglected. τ is expressed as:

$$\tau = \frac{3\alpha}{c_s^2 \Delta t} + \frac{1}{2} \tag{13}$$

The local equilibrium energy distribution function g_k^{eq} is written as follow:

$$g_k^{eq} = w_k T \left[1 + 3\frac{c_k u^{eq}}{c^2} \right] \tag{14}$$

According to that, the fluid temperature $T(x,t)$ can be evaluated by:

$$T(x,t) = \sum_{k=0}^{8} g_k(x,t) \tag{15}$$

For LBM modelling of NC, the buoyancy force term is given by:

$$F_k = \frac{w_k \rho g \beta (T - T_c)}{c_s^2} \left(c_{k,x} \sin(\Omega) + c_{k,y} \cos(\Omega) \right) \tag{16}$$

2.3. Nusselt number calculation

The dimensionless Nusselt number (Nu) performs the evaluation of natural convective heat transfer for a fluid flow. This number defines the dominance of convection compared to conduction. The following expressions are used for a better estimation:

1- Average Nusselt number for the cold wall:

$$\overline{Nu_C} = -\frac{1}{L(T_h - T_c)} \int_0^L k \frac{\partial T}{\partial x} dy \tag{17}$$

2- Average Nusselt number for sinks:

$$\overline{Nu_C} = -\frac{1}{(L_b + 2h_b)(T_h - T_c)} \int_0^{L_b + 2h_b} k \frac{\partial T}{\partial n} dl \tag{18}$$

3- Average Nusselt number for sources:

$$\overline{Nu_H} = -\frac{1}{(L_b + 2h_b)(T_h - T_c)} \int_0^{L_b + 2h_b} k \frac{\partial T}{\partial n} dl \tag{19}$$

2.4. Numerical implementation

The incompressible regime imposes a value of Mach number lower than 0.3. Hence, for our code to be implemented, it must meet this condition. In this study, the value of 0.1 has been assigned to the Mach number. Based on this logic, the viscosity could be estimated, depending on the parameters governing the problem, by [56]:

$$\vartheta = \sqrt{\frac{PrMa^2 M^2 c_s^2}{Ra}} \tag{20}$$

2.5. Grid sensitivity study and code validation

The sensitivity of the results to the grid size was executed by considering four different grid sizes. The four grid sizes of 200×100, 300×150, 400×200 and 500×250 are used. The results are associated to the case 1 with different inclinations. Table 1 shows the results obtained with respect to the value of the stream function at the centre of the enclosure. A quick analysis of the data shown in Table 1 could help us to choose the grid size 400×200 due to the low deviation after passing through the next grid size of 500×250 and which is equal to 1.05% and 1.41% for an inclination of 90° and 0°, respectively. Indeed, this grid size is sufficient to give accurate results. Other grid sizes could be adopted but they require a drastic CPU time without improvement of the computational accuracy and no optimization of the computational time could be reported.

To validate our in-house FORTRAN-LBM code, the latter has been modified to reproduce the same problem treated by De Vahl Davis [57]. The numerical predictions obtained by our code were compared to the numerical results of Ref. [57] in terms of isotherms for $Ra = 10^5$. Fig. 3 displays a very good agreement between the results. A quantitative validation was also performed by comparing the average Nu values and maximum dimensionless velocities along the vertical and horizontal centerline obtained by our code and those from different works in the literature. Tables 2 and 3 gather the obtained results, which also confirms a sufficient agreement.

A second validation study was performed by comparing our results with those obtained by COMSOL Multiphysics software. An attempt was

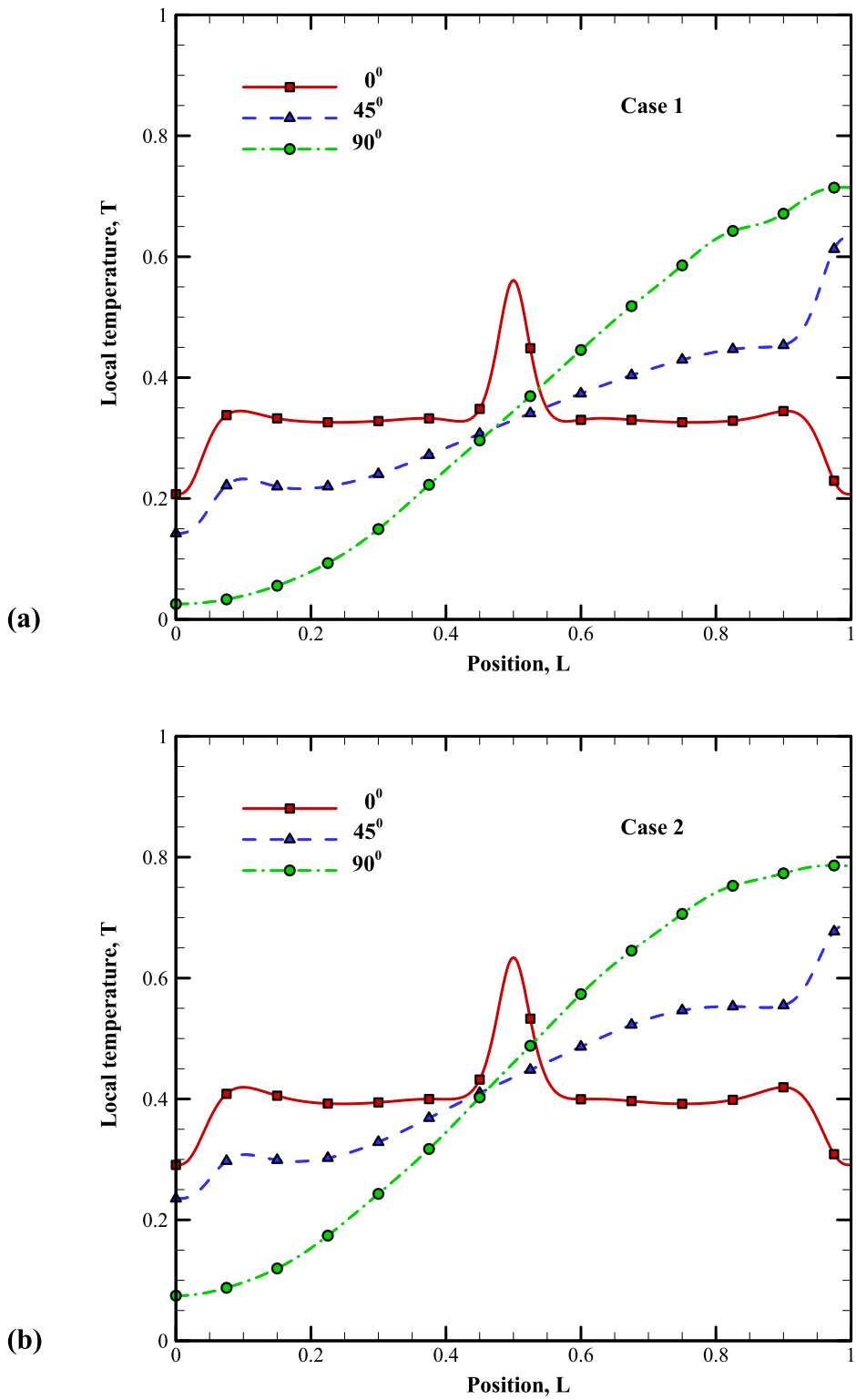

Fig. 12. Local temperature distribution along the central line for $Ra = 10^6$.

made to reproduce the same problem of case 1 of the present study in the commercial software with an inclination of 0^0 for $Ra = 10^3$ and $Ra = 10^5$. The results obtained were presented in terms of isotherms and streamlines for each value of Rayleigh number as shown in Fig. 4. An excellent agreement between the two results could be observed.

3. Results and discussion

3.1. General trends of isotherms and fluid flow pattern

The isotherms and streamlines are depicted in Figs. 5–8 for the two investigated cases (case 1 and case 2) and three tilt angles ($\Omega = 0°$, 45°, and 90°) considering four different values of Rayleigh number (10^3, 10^4, 10^5, and 10^6). For $Ra = 10^3$, the heat transfer is driven mainly by

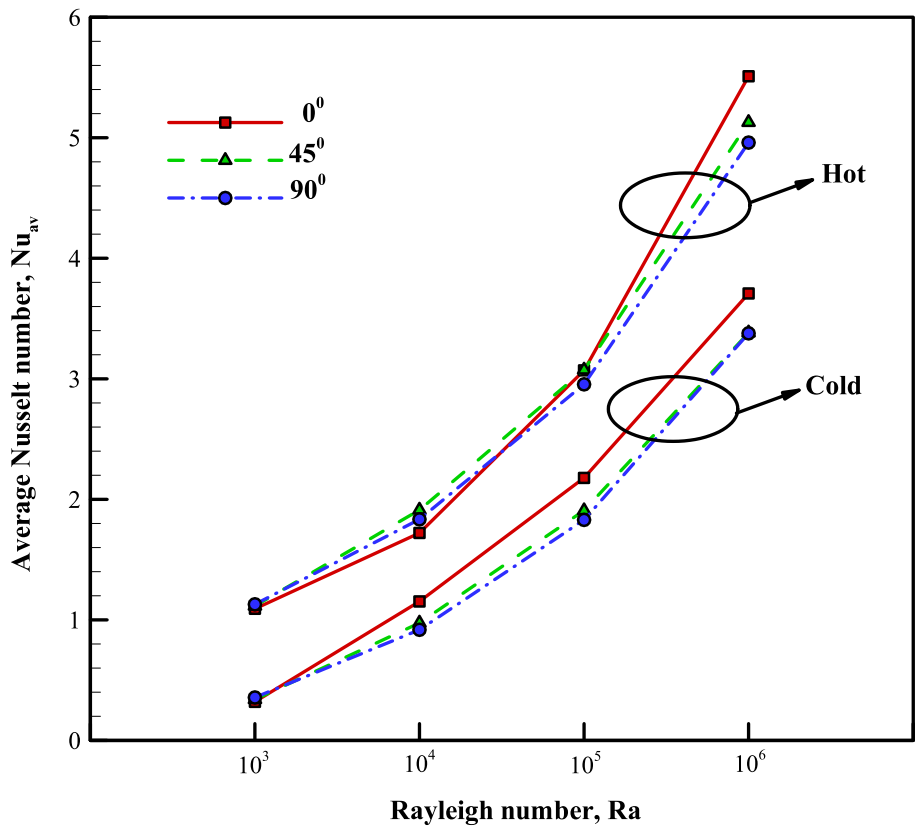

Fig. 13. Average Nusselt number dependency on Rayleigh number for case 1.

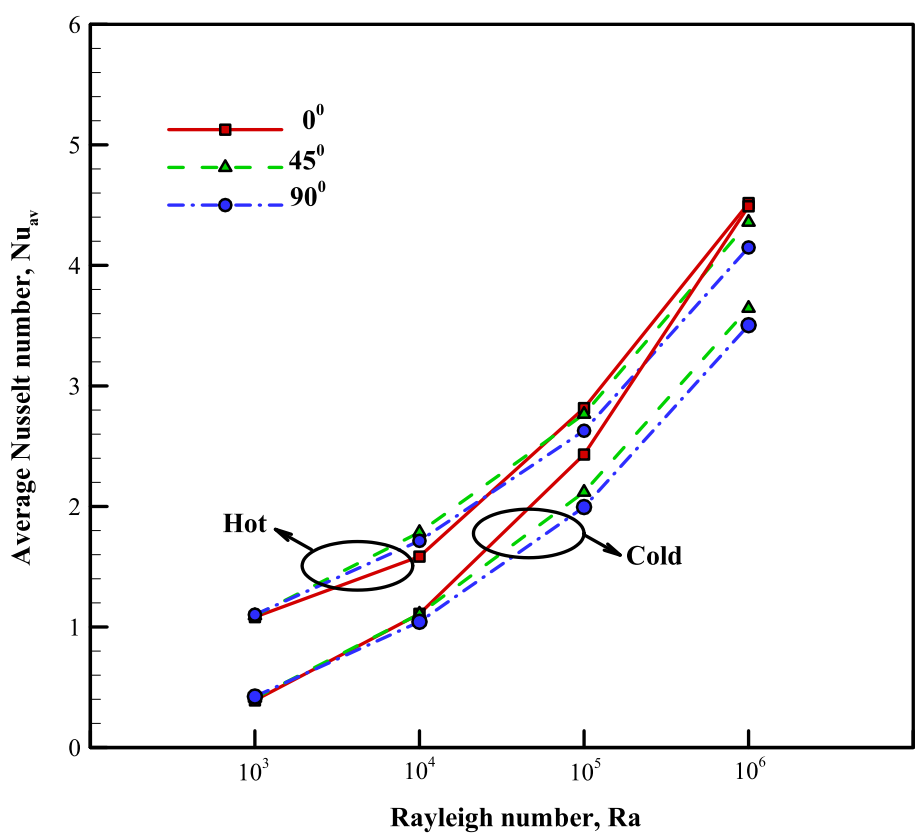

Fig. 14. Average Nusselt number dependency on Rayleigh number for case 2.

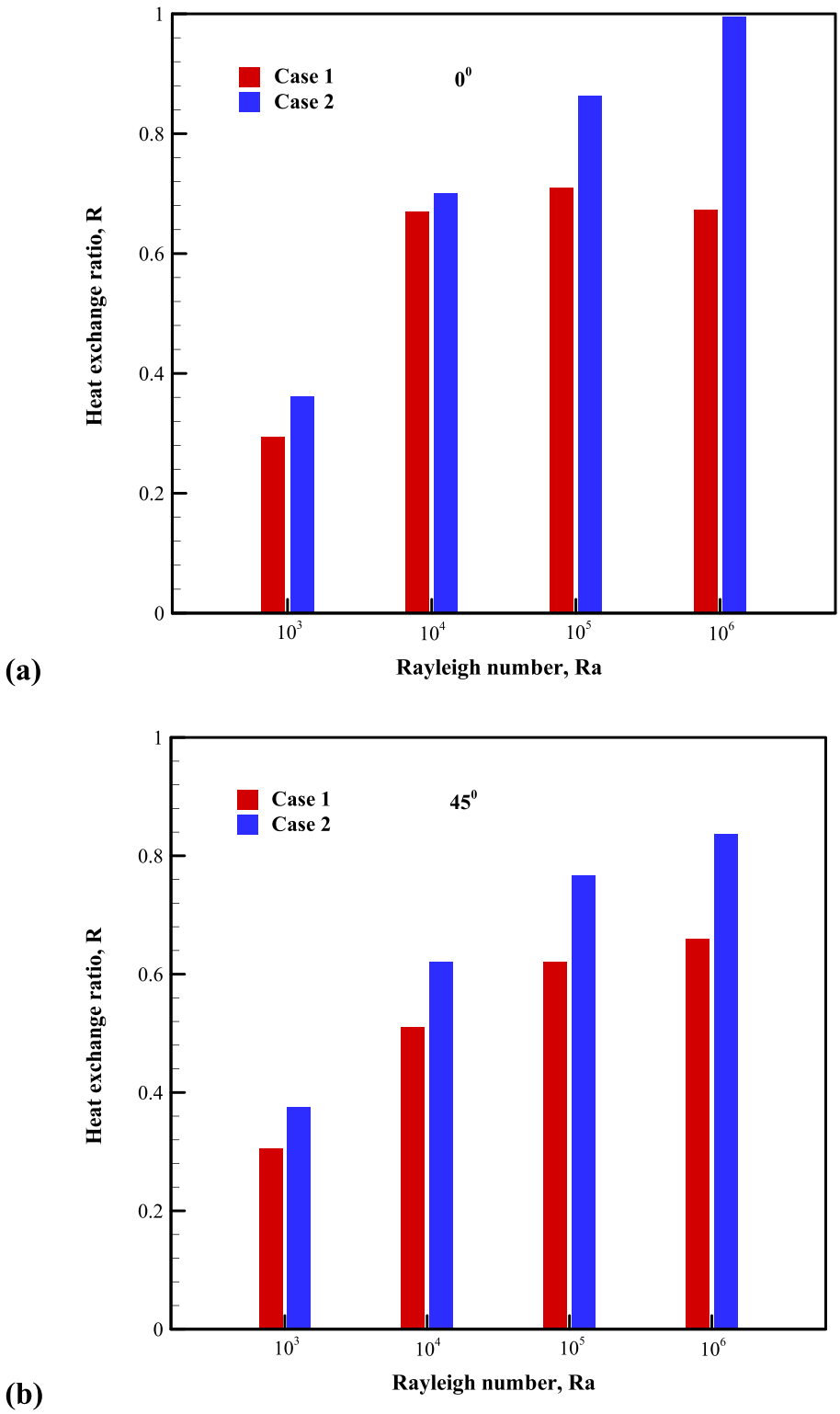

Fig. 15. Heat exchange ratio dependency on Rayleigh number for an inclination of (a) 0°, (b) 45°, and (c) 90°.

conduction as indicated by the nearly isotherms (Fig. 5) for the two studied cases and all tilt angles. The streamlines show one large dominant counter-clockwise cell except the horizontal position $\Omega = 0°$ for and this for both cases (case 1 and case 2) where two main counter-rotating vortices characterize the coolant flow structure. Increasing Ra to $Ra = 10^4$ results in distorted streamlines for all cases (Fig. 6) meaning heat transfer dominated by convection at this case. The heat transfer in the enclosed fluid becomes governed by NC heat transfer which induces fluid circulation caused by the buoyancy effect inside the enclosure. When Ra increases, temperature differences are higher inducing convective flow which results in temperature peaks observed according to the enclosure inclination. A thermal plume appears in the horizontal cavity for both cases 1 and 2. With further increase in Ra i.e., $Ra = 10^5$, illustrated in Fig. 7, the streamlines become more denser with increasing

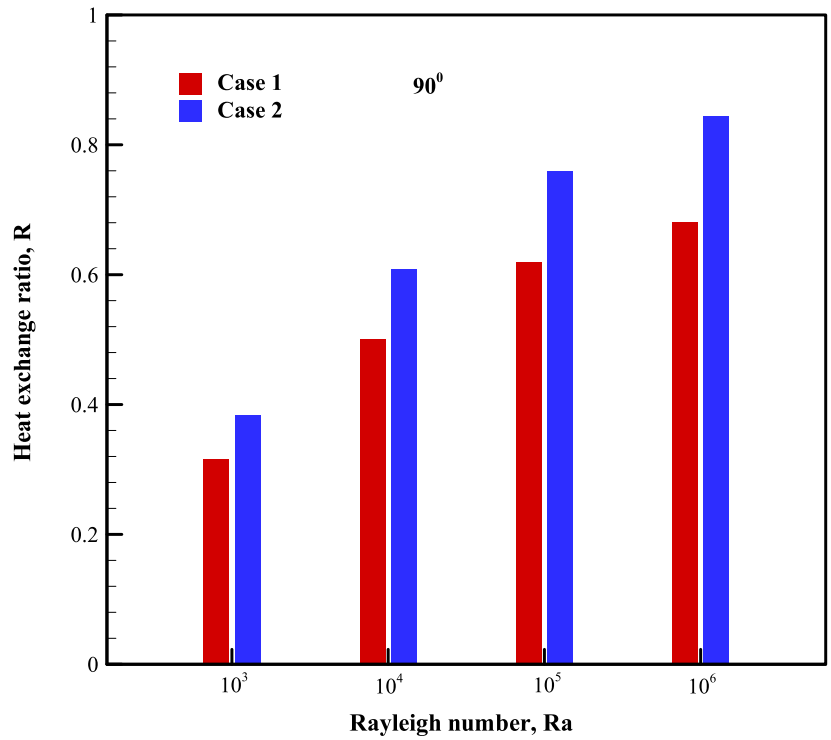

(c)

Fig. 15. (*continued*).

intensity of NC heat transfer, mainly near the heating components. The upper fluid circulation is stronger than that the above one inside the 45°-cavity. The maximum streamline function values obtained for the case 1 are 4.5, 7.12, 7.71 for $\Omega = 90°$, 45°, and 0°, respectively, while for the case 2, the maximum computed values are 3.97, 6.15, 6.65 for $\Omega = 90°$, 45°, and 0°, respectively. Fig. 8 shows the simulations in the case of higher value of Ra ($Ra = 10^6$). New vortices appear in the enclosures for both case 1 and 2 due to the strong intensity of NC heat transfer. The flow structure changes, the plume in the horizontal cavity is split into two parts due to the active fluid flow induced by buoyancy. The streamline's function indicates maximum values for case 1: 8.55, 12.22, 22.77, for $\Omega = 90°$, 45°, and 0°, respectively, and for case 2, values of 7.47, 10.69, 18.5 for $\Omega = 90°$, 45°, and 0°, respectively. Among all inclinations, the horizontal position shows the most significant natural convective flow in the enclosure. This effect is more pronounced in the case 2 as compared to the case 1 where the air near the hot sources at the bottom is heated and raised upward due to the buoyancy force for a short path to cool down on the upper cold wall and return backward.

3.2. Temperature profiles

The temperature profile along the centreline of the cavity is illustrated in Figs. 9–12 for case 1 and case 2, three tilt angles ($\Omega = 0°$, 45°, and 90°) and different Rayleigh numbers ranging from 10^3 to 10^6. Fig. 9 shows the temperature profiles in the investigated cavities (case 1 and case) at $Ra = 10^3$ for the three inclinations (0°, 45°, and 90°). Due to the low Ra, the overall temperature rise is not significant for $Ra = 10^3$ as shown in Fig. 9. The significant overheating is observed for $Ra \geq 10^4$. Similar trends in temperature profile are found for $Ra = 10^3$ in the two cases i.e., uniform cold wall (case 1)/discrete twin cold components (case 2). Due to the low heat transfer dominated mainly by conduction the enclosures do not overheat where the maximal temperature (dimensionless) observed lie between 0.4 and 0.45. The temperature distribution does not show significant difference between the two cases 1 and 2 in a hand and on the other hand within the same enclosure. The higher temperatures are shown in the middle of the enclosure above the two heat sources for the horizontal enclosure, where a symmetry in the temperature profile is obtained while high temperatures are shown in the top half of the enclosure for both inclinations 45° and 90°. The horizontal enclosure shows symmetry in the temperature profile with respect to the vertical centreline, whereas 45° and 90°-inclined cavities show peaks in the top half of the enclosure caused by the weak fluid circulation. Similar temperature profiles are shown in the two inclined cavities except the slight difference shown on the top due to the pattern of the nature of the weak convective currents. It is worth noting that at $Ra = 10^3$, the temperature profile is not affected by the cooling configuration either uniform cold wall (case 1) and discrete twin sinks (case 2) show the same temperature profile. Besides, at low Ra i.e., low heat dissipation the horizontal enclosure observes slightly low overheating effect compared to the inclined cavities. The highest temperature is obtained in the case of 90° tilt followed by the 45° case.

The temperature profiles in the investigated cavities (case 1 and case 2) at $Ra = 10^4$ is plotted in Fig. 10 for $\Omega = 0°$, 45°, and 90°. The temperature profiles show significant change caused by the significant NC heat transfer, which affects the fluid flow pattern. The horizontal cavity presents a symmetrical profile with noticeable temperature peak 0.75 (dimensionless) above the centre i.e. conjugate effect of heat dissipated between the two heat sources. Similar trends are found in the two remaining inclinations (45° and 90°) with slight advantage of the former in terms of low overheating inside the cavity. These two inclinations show increasing temperature along L with temperature peaks 0.72 and 0.73 comparable in value with that obtained for $\Omega = 0°$. Unlike the previous simulations with $Ra = 10^3$, the peaks are located on the upper wall which means quasi-stratified temperatures within the inclined enclosures. It is noted that the configuration (i.e., cold wall/ twin cold protruding components) does not affect the temperature profile as both Fig. 10a and b show similar trends for all inclinations at $Ra = 10^4$. This similar behavior is also found with lower Rayleigh number (Fig. 9).

As Ra is increased ($Ra = 10^5$ and $Ra = 10^6$, Figs. 11 and 12, respectively), there is no significant difference between the effect of $Ra = 10^5$ and $Ra = 10^6$ on the temperature's profiles of all simulated

cases. For $Ra = 10^5$, the temperature profiles become much more complicated, mainly for the $\Omega = 0^\circ$ and 45°, due to the strong NC heat transfer currents. Nonetheless, the 90°-enclosure keeps roughly the same increasing temperature trend along the cavity due to the vertical active walls, which are parallel to the gravity. The 45°-inclined cavity keeps temperature increasing along the cavity but with different rates; the steeper is shown on the top half of the cavity to achieve a peak on the top wall. This steepness is explained by the stronger upper vortex compared to the lower one shown in Fig. 7. The peak is on the top wall not below as shown previously for lower *Ra*. For $Ra > 10^4$, the cavity overheating in the horizontal cavity is observed at the middle above the space between the two heating components. For the remaining two cavities i.e., the vertical and inclined enclosure, the overheated area is located at the top of the cavity with higher temperatures in the case of the vertical position.

3.3. Heat transfer analysis

3.3.1. Average Nusselt number

Thermal performance of the simulated configurations is compared by means of the $\overline{Nu}$ on both cold and hot walls. Figs. 13 and 14 depict the effect of *Ra* on the $\overline{Nu}$ on both active walls i.e. cold and hot wall and this for the enclosure tilts 0°, 45°, and 90°, for both case 1 and case 2. First of all, we note that $\overline{Nu}$ increases with increasing *Ra* for all configurations, this increment is more noticeable with strong NC heat transfer. The maximum $\overline{Nu} = 5.51$ is obtained on the hot wall for the horizontal cavity in the case of cold uniform wall (case 1) for $Ra = 10^6$. On the hand, the cavity tilt significantly affects the heat transfer rate. This effect is more pronounced in the case of horizontal enclosure that shows higher $\overline{Nu}$ values compared to the two remaining inclinations, mainly for high *Ra* numbers where the buoyancy force is significant. Regarding the cavity tilt, the $\overline{Nu}$ is higher in the case of a horizontal enclosure followed by the 45°-inclined-enclosure and finally the vertical cavity. This is due to the buoyancy force effect where this effect is favourable for the two former inclinations (i.e., 90° and 45°) regarding the position of the hot sources which enables rapid hot–cold surface heat transfer process, due to the short distance when compared to the vertical enclosure. In fact, the hot air in the latter vertical enclosure travels upward along the hot surface and downward along the cold surface which results in lower heat transfer rate and hence lower $\overline{Nu}$ values when compared to the two other cavity tilts. However, the difference between the $\overline{Nu}$ values become more significant as *Ra* increases due to the strong fluid convective circulation resulting in a high transfer rate. In contrary, for low values of *Ra*, there is no significant effect of *Ra* on the $\overline{Nu}$ and this for all simulated configurations. Furthermore, on the hot wall, there is no significant effect of the enclosure tilt on the $\overline{Nu}$ for $Ra \leq 10^5$ and this apply for the two cases i.e., case 1 and case 2. The $\overline{Nu}$ on the cold wall is higher for the horizontal enclosure in comparison to the other two inclinations for all *Ra* numbers whereas on the hot wall the $\overline{Nu}$ is higher in the case of the horizontal cavity position for only high values of *Ra* i.e., $Ra > 10^5$.

For the discrete cold protruding (case 2), heat transfer rate on the cold wall is higher for the horizontal position when $Ra > 10^4$ while no significant difference is observed for lower *Ra* values. On the hot wall a much-complicated behaviour is shown for heat transfer in the cavity. For $Ra > 10^5$, the horizontal cavity outperforms the other cavities in terms of heat transfer rate, but this position is the less performant for $Ra < 10^4$. The inversion of this behaviour should take place midway between $Ra = 10^4 \text{and} 10^5$.

3.3.2. Heat exchange ratio

For a more detailed heat transfer analysis, a heat exchange ratio *R* is introduced. This is a quantity representing the ratio between the average Nusselt number in vicinity of the cold part (sinks) $\overline{Nu}_C$ and the average Nusselt number in vicinity of the hot part (heat sinks)$\overline{Nu}_H$ ($R = \frac{\overline{Nu}_C}{\overline{Nu}_H}$). In other words, *R* is a parameter reflecting the rate of heat transfer between the two different regions. Consequently, a high heat exchange ratio characterizes better heat dissipation. At this stage, it could be argued that the average Nusselt number and the heat exchange ratio are two decisive parameters for determining the optimal configuration. Fig. 15 shows the evolution of the heat exchange ratio *R* as a function of Rayleigh number and heat sink inclination, for cases 1 and 2.

Equipping the cavity with a twin sinks (case 2) instead of a cold wall (case 1) reduces heat transfer by inducing an apparent drop in the Nusselt number, see Figs. 13 and 14. Evaluating only the average Nusselt number, we cannot judge which configuration is recommended for better evacuation of the heat generated by electronic components in ON state. The difference in values between the average Nusselt number in vicinity of the hot and cold sides leads us to the introduction of the heat exchange ratio R. This difference is due, firstly, to the fact that we have considered protruding electronic components occupying a space in the air-filled cavity. Secondly, there is the mechanical reason that the protruding electronic components act as an obstacle to fluid flow, delaying its movement. It could also be justified from a thermal point of view, as heat exchange takes place by conduction within the electronic components on the one hand and by NC between the electronic components and the fluid on the other. This contributes to a reduction in heat flow between the hot/cold part and the surrounding fluid.

Looking at Fig. 15, it is clear that, for all inclination values, the heat exchange ratio increases as the Rayleigh number increases, whatever the case. Moreover, in all cases, the heat exchange ratio evaluated in case 2 is high compared to that evaluated in case 1. A maximum value of 0.99 is highlighted for case 2 with an inclination of 0° and $Ra = 10^6$. For the same configuration and conditions, this value is 0.67 in case 1. By replacing the cold wall (case 1) with a twin sinks (case 2), the heat exchange ratio is improved by 32.32 %. This is the configuration with the best heat dissipation.

4. Conclusions

Natural convection of air inside a cavity embedded with simultaneous presence of a twin heat sources (representing protruding electronic components) and a twin sinks/isothermal cold wall is simulated using the lattice Boltzmann method. The effect of the enclosure inclination (0°, 45°, and 90°) on the thermal and dynamic field is studied for different *Ra* ranging from $10^3 \text{to} 10^6$. The enclosure could be cooled by either a uniform cold wall maintained at a constant temperature T_c (case 1) or a sink pair maintained at a constant temperature T_c (cases 2); "OFF" state. The following conclusions are drawn:

- Smooth thermal and dynamic fields are obtained at low *Ra* values.
- At high *Ra* number, the buoyancy driven natural convection is significantly active; the vertical enclosure shows the most noticeable overheating at the top of the cavity, followed by 45° inclined cavity also at the top, and lastly the horizontal cavity, however the overheating in the latter cavity is shown at the middle above the space between the two heat sources.
- For the uniform top cold wall (case 1), the heat transfer rate on the cold wall is higher for the horizontal position compared to the inclined cavities and this effect apply for all investigated *Ra* values but the heat transfer on the cold wall is higher for the vertical position for only $Ra > 10^5$.
- For case 1, the heat transfer is improved by 80% by varying the Rayleigh number *Ra* from 10^3 to 10^6 with a horizontal disposition.
- For case 2, i.e., twin cold protruding, heat transfer rate on the hot wall shows a complicated behaviour. For $Ra > 10^5$, the horizontal cavity outperforms the other cavities in terms of heat transfer rate, but the horizontal position is the less performant for $Ra < 10^4$.

- Results indicate no significant difference of the average $\overline{Nu}$ computed for the two inclined cavities i.e., 45° and 90° for both cases regardless the Ra value.
- The maximal heat transfer rate corresponding to $\overline{Nu} = 5.51$ is obtained on the hot wall for the horizontal cavity in the case of a cold uniform wall (case 1) for $Ra = 10^6$.
- With a horizontal disposition and $Ra = 10^6$, the heat exchange ratio is improved by 32.32 % in case 2 compared to case 1.
- The second configuration is recommended for the best heat dissipation.

For future research, we will consider multiple heat sources/sinks of various shapes, sizes, and positions. Despite the increasing use of the LBM method for the numerical solution of heat and mass transfer problems, this technique has certain limitations. The major limitation is the simulation of high Mach number flows for aerodynamic applications. To date, no thermo-hydrodynamic scheme has been proposed to overcome this limitation.

CRediT authorship contribution statement

Hamza Faraji: Conceptualization, Methodology, Software, Data curation, Formal analysis, Writing – original draft, Writing – review & editing, Visualization. **Mohamed Teggar:** Formal analysis, Writing – review & editing, Visualization. **Adeel Arshad:** Formal analysis, Writing – review & editing, Visualization. **Müslüm Arıcı:** Formal analysis, Investigation, Writing – original draft, Writing – review & editing. **El Mehdi Berra:** Writing – review & editing, Visualization. **Khadija Choukairy:** Writing – review & editing, Visualization.

Declaration of Competing Interest

The authors declare that they have no known competing financial interests or personal relationships that could have appeared to influence the work reported in this paper.

Data availability

Data will be made available on request.

References

[1] B. Adrian, Convection Heat Other Books by Adrian Bejan, John Wiley & Sons Inc,, 2013.
[2] H. Buchberg, I. Catton, D. Edwards, Natural convection in enclosed spaces—a review of application to solar energy collection, 1976.
[3] A. Rahimi, A. Dehghan Saee, A. Kasaeipoor, E. Hasani Malekshah, A comprehensive review on natural convection flow and heat transfer: the most practical geometries for engineering applications, Int. J. Numer. Meth. Heat Fluid Flow 29 (3) (2019) 834–877.
[4] H. Faraji, M.E. Alami, A. Arshad, Y. Hariti, Numerical survey on performance of hybrid NePCM for cooling of electronics: effect of heat source position and heat sink inclination, J. Therm. Sci. Eng. Appl. 13 (5) (2021) 1–30, https://doi.org/10.1115/1.4049431.
[5] H. Faraji, M. Faraji, M. El Alami, Y. Hariti, A. Arshad, A. Hader, A. Benkaddour, Cooling of recent microprocessors by the fusion of nano-enhanced phase change materials, Mater. Today:. Proc. 30 (2020) 865–869, https://doi.org/10.1016/j.matpr.2020.04.342. Elsevier Ltd.
[6] Z. He, Y. Yan, Z. Zhang, Thermal management and temperature uniformity enhancement of electronic devices by micro heat sinks: a review, Energy 216 (2021), 119223.
[7] A. Arshad, et al., Cooling performance of an active-passive hybrid composite phase change material (HcPCM) finned heat sink: constant operating mode, Int. J. Heat Mass Transf. 207 (2023), 123973.
[8] J. Mathew, S. Krishnan, A Review on transient thermal management of electronic devices, J. Electron. Packag. 144 (1) (2021).
[9] Y. Liu, R. Zheng, J. Li, High latent heat phase change materials (PCMs) with low melting temperature for thermal management and storage of electronic devices and power batteries: critical review, Renew. Sustain. Energy Rev. 168 (2022), 112783.
[10] I. Afaynou, et al., Heat transfer enhancement of phase-change materials (PCMs) based thermal management systems for electronic components: a review of recent advances, Int. Commun. Heat Mass Transf. 143 (2023), 106690.
[11] Y. Ma, R. Mohebbi, M.M. Rashidi, Z. Yang, M.A. Sheremet, Numerical study of MHD nanofluid natural convection in a baffled U-shaped enclosure, Int. J. Heat Mass Transf. 130 (2019) 123–134.
[12] A.T. Franco, et al., The effects of discrete conductive blocks on the natural convection in side-heated open cavities, Appl. Therm. Eng. 219 (2023), 119613.
[13] S.A. Khan, et al., CFD simulation and optimization of natural convection in a vertical annulus with nanofluids, Int. J. Therm. Sci. 185 (2023), 108079.
[14] K. Wang, et al., A numerical study on the natural convective heat loss of an isothermal upward-facing cylindrical cavity, Appl. Therm. Eng. 213 (2022), 118763.
[15] S.D. Farahani, A.D. Farahani, H.F. Öztop, Natural convection in a rectangular tall cavity in the presence of an oscillating and rotating cylinder, Colloids Surf. A Physicochem. Eng. Asp. 647 (2022), 129027.
[16] S. Baghsaz, S. Rezanejad, M. Moghimi, Numerical investigation of transient natural convection and entropy generation analysis in a porous cavity filled with nanofluid considering nanoparticles sedimentation, J. Mol. Liq. 279 (2019) 327–341.
[17] A.S. Gawas, D.V. Patil, Natural convection heat transfer with anisotropic thermal diffusion for tilted two-dimensional cavities, Int. J. Heat Mass Transf. 194 (2022) 123000.
[18] F. Selimefendigil, H.F. Öztop, Natural convection and entropy generation of nanofluid filled cavity having different shaped obstacles under the influence of magnetic field and internal heat generation, J. Taiwan Inst. Chem. Eng. 56 (2015) 42–56.
[19] M. Sheikholeslami, M. Gorji-Bandpy, S.M. Seyyedi, D.D. Ganji, H.B. Rokni, S. Soleimani, Application of LBM in simulation of natural convection in a nanofluid filled square cavity with curve boundaries, Powder Technol. 247 (2013) 87–94.
[20] Y. Ma, R. Mohebbi, M.M. Rashidi, Z. Yang, Simulation of nanofluid natural convection in a U-shaped cavity equipped by a heating obstacle: effect of cavity's aspect ratio, J. Taiwan Inst. Chem. Eng. 93 (2018) 263–276.
[21] H. Daghab, M. Kaddiri, S. Raghay, I. Arroub, M. Lamsaadi, H. Rayhane, Finite volume simulation of natural convection for power-law fluids with temperature-dependent viscosity in a square cavity with a localized heat source, Int. J. Heat Technol. 39 (5) (2021) 1405–1416.
[22] R. Hidki, et al., Impact of Cu, Al_2O_3-water hybrid nanofluid on natural convection inside a square cavity with two heat-generating bodies, Mater. Today:. Proc. 72 (2023) 3749–3756.
[23] I. Arroub, et al., Heat transfer performance in a tilted cavity submitted to external flow of nanofluid, in: AIP Conference Proceedings, AIP Publishing.
[24] J. Benhamou, E.B. Lahmer, M. Jami, M.A. Moussaoui, A. Mezrhab, 3D numerical investigation of free convection using lattice Boltzmann and finite difference methods, Int. J. Renew. Energy Dev. 11 (4) (2022) 916–925.
[25] S.K. Saha, Numerical study of laminar natural convection heat transfer in inclined trapezoidal enclosure, J. Therm. Sci. Eng. Appl. 11 (6) (2019), 061021.
[26] F. Zemani, A. Sabeur, Computational fluid dynamics-based analysis of entropy generation on laminar natural convection in enclosures with partitioned walls and for different heating positions, J. Heat Transf. 144 (6) (2022), 062601.
[27] J. Alinejad, J.A. Esfahani, Lattice Boltzmann simulation of forced convection over an electronic board with multiple obstacles, **45**(3) (2014) 241–262.
[28] J. Alinejad, J.A. Esfahani, Numerical stabilization of three-dimensional turbulent natural convection around isothermal cylinder, J. Thermophys. Heat Transfer. 30 (1) (2015) 94–102.
[29] S.M. Moafi Madani, et al., Numerical study of geometric parameters effects on the suspended solid particles in the oil transmission pipelines, Proc. Inst. Mech. Eng. C J. Mech. Eng. Sci. 236 (8) (2021) 3960–3973.
[30] J. Alinejad, Lattice Boltzmann simulation of a fluid flow around a triangular unit of three isothermal cylinders, J. Appl. Mech. Tech. Phys. 57 (1) (2016) 117–126.
[31] R. Djebali, M. Ferhi. Appraising heat transfer enhancement by nanofluid and entropy generation minimization in a micro tall cavity: : magnetic field and sinusoidal heating effects, in: 2022 13th International Renewable Energy Congress (IREC), 2022.
[32] M. Ferhi, R. Djebali, Appraising conjugate heat transfer, heatlines visualization and entropy generation of Ag-MgO/HO hybrid nanofluid in a partitioned medium, Int. J. Numer. Meth. Heat Fluid Flow 30 (10) (2020) 4529–4562.
[33] M. Ferhi, R. Djebali, W. Al-Kouz, S. Abboudi, A.J. Chamkha, MHD conjugate heat transfer and entropy generation analysis of MWCNT/water nanofluid in a partially heated divided medium, Heat Transf. 50 (1) (2021) 126–144.
[34] R. Djebali, M. Ferhi, DOE of heat transfer and entropy generation in channel microheat exchanger driven by a coflow, in: 2022 13th International Renewable Energy Congress (IREC), 2022.
[35] D. Das, M. Roy, T. Basak, Studies on natural convection within enclosures of various (non-square) shapes – a review, Int. J. Heat Mass Transf. 106 (2017) 356–406, https://doi.org/10.1016/J.IJHEATMASSTRANSFER.2016.08.034.
[36] S. Husain, S.A. Khan, A review on heat transfer enhancement techniques during natural convection in vertical annular geometry, Clean. Eng. Technol. 5 (2021) 100333, https://doi.org/10.1016/J.CLET.2021.100333.
[37] A. Abdulkadhim, I.M. Abed, N.M. Said, An exhaustive review on natural convection within complex enclosures: influence of various parameters, Chin. J. Phys. 74 (2021) 365–388.
[38] A.H. Majeed, et al., Heat and mass transfer characteristics in MHD Casson fluid flow over a cylinder in a wavy channel: higher-order FEM computations, Case Stud. Therm. Eng. 42 (2023), 102730.
[39] F. Qin, Q.i. He, Y. Gong, T. An, P. Chen, Y. Dai, The application of FEM-BEM coupling method for steady 2D heat transfer problems with multi-scale structure, Eng. Anal. Bound. Elem. 137 (2022) 78–90.

[40] M. Sheikholeslami, A. Ghasemi, Solidification heat transfer of nanofluid in existence of thermal radiation by means of FEM, Int. J. Heat Mass Transf. 123 (2018) 418–431.
[41] K. Muhammad, et al., Squeezed flow of MHNF (modified hybrid nanofluid) with thermal radiation and CC (Cattaneo-Christov) heat flux: a numerical study via FDM, Mater. Sci. Eng. B 289 (2023), 116268.
[42] K. Muhammad, T. Hayat, S. Momani, S. Asghar, FDM analysis for squeezed flow of hybrid nanofluid in presence of Cattaneo-Christov (CC) heat flux and convective boundary condition, Alex. Eng. J. 61 (6) (2022) 4719–4727.
[43] H.M. Patil, R. Maniyeri, Finite difference method based analysis of bio-heat transfer in human breast cyst, Therm. Scie. Eng. Prog. 10 (2019) 42–47.
[44] M.-J. Li, et al., An efficient and high-fidelity local multi-mesh finite volume method for heat transfer and fluid flow problems in metal additive manufacturing, Comput. Methods Appl. Mech. Eng. 404 (2023), 115828.
[45] A. Arshad, et al., Thermal process enhancement of HNCPCM filled heat sink: effect of hybrid nanoparticles ratio and shape, Int. Commun. Heat Mass Transf. 125 (2021), 105323.
[46] N. Abouricha, M. El Alami, K. Souhar, Lattice Boltzmann modeling of convective flows in a large-scale cavity heated from below by two imposed temperature profiles, HFF 30 (5) (2020) 2759–2779, https://doi.org/10.1108/HFF-12-2018-0823/FULL/XML.
[47] Y. Dahani, M. Hasnaoui, A. Amahmid, S. Hasnaoui, A. El Mansouri, I. Filahi, Numerical analysis of heat transfer evacuation from a cavity confining coated micro-pin fin heat sink using lattice Boltzmann approach, Eur. Phys. J. Plus 137 (5) (2022), https://doi.org/10.1140/EPJP/S13360-022-02789-2.
[48] A. Laouer, M. Arıcı, M. Teggar, S. Bouabdallah, Ç. Yıldız, K.A.R. Ismail, S.S. M. Ajarostaghi, E.H. Mezaache, Effect of magnetic field and nanoparticle concentration on melting of Cu-ice in a rectangular cavity under fluctuating temperatures, J. Storage Mater. 36 (2021) 102421, https://doi.org/10.1016/J.EST.2021.102421.
[49] M. Ouahas, A. Amahmid, M. Hasnaoui, A.E. Mansouri, Y. Dahani, Multi relaxation time lattice Boltzmann method simulation of natural convection combined with surface radiation in a square open cavity from three discrete heat sources, Heat Transf. Eng. 42 (8) (2021) 706–722.
[50] U. Frisch, B. Hasslacher, Y. Pomeau, Lattice-gas automata for the Navier-Stokes equation, Phys. Rev. Lett. 56 (14) (1986) 1505–1508.
[51] U. Frisch, Relation between the lattice Boltzmann equation and the Navier-stokes equations, Physica D 47 (1-2) (1991) 231–232, https://doi.org/10.1016/0167-2789(91)90293-I.
[52] F.J. Higuera, J. Jiménez, Boltzmann Approach to Lattice Gas Simulations, Europhys. Lett. 9 (7) (1989) 663–668, https://doi.org/10.1209/0295-5075/9/7/009.
[53] H. Chen, S. Chen, W.H. Matthaeus, Recovery of the Navier-Stokes equations using a lattice-gas Boltzmann method, Phys. Rev. A 45 (8) (1992) R5339–R5342, https://doi.org/10.1103/PhysRevA.45.R5339.
[54] Y. Yan, Y. Zu, Numerical simulation of heat transfer and fluid flow past a rotating isothermal cylinder–a LBM approach, Int. J. Heat Mass Transf. 51 (9–10) (2008) 2519–2536.
[55] E.M. Berra, M. Faraji, H. Faraji, Numerical simulation with LBM of the cooling of electronic component: effect of the inclination angle, Mater. Today: Proc. 30 (2019) 838–841, https://doi.org/10.1016/j.matpr.2020.04.194.
[56] A. Mohamad, A. Kuzmin, A critical evaluation of force term in lattice Boltzmann method, natural convection problem, Int. J. Heat Mass Transf. 53 (5–6) (2010) 990–996.
[57] G. de Vahl Davis, Natural convection of air in a square cavity: a bench mark numerical solution, Int. J. Numer. Meth. Fluids 3 (3) (1983) 249–264.
[58] K. Khanafer, K. Vafai, M. Lightstone, Buoyancy-driven heat transfer enhancement in a two-dimensional enclosure utilizing nanofluids, Int. J. Heat Mass Transf. 46 (19) (2003) 3639–3653.
[59] T. Fusegi, J.M. Hyun, K. Kuwahara, B. Farouk, A numerical study of three-dimensional natural convection in a differentially heated cubical enclosure, Int. J. Heat Mass Transf. 34 (6) (1991) 1543–1557.